Publications of the Astronomical Society of the Pacific
107: 966–976, 1995 October

Determining Spectrometer Instrumental Profiles Using FTS Reference Spectra[1]

JEFF A. VALENTI

JILA, University of Colorado, Boulder, Colorado 80309
Electronic mail: jvalenti@casa.colorado.edu

R. PAUL BUTLER[2] AND GEOFFREY W. MARCY[2]

Astronomy Department, University of California, Berkeley, California 94720
Electronic mail: gmarcy@etoile.berkeley.edu, paul@further.berkeley.edu

Received 1995 May 12; accepted 1995 July 11

ABSTRACT. We describe a new technique for determining the instrumental profile (IP) of an astronomical spectrometer. A known intrinsic spectrum of a reference source is convolved with a parameterized IP and then compared to a spectrum obtained with the spectrometer to be characterized. Nonlinear least-squares (NLLS) optimization is used to solve for the analytic IP that best reproduces the observed spectrum. This technique is most effective for characterizing the central portion of the IP, out to 1% of the peak. IP recovery is demonstrated using both the Sun and an I_2 absorption cell as reference spectra. We also describe a second technique employing singular value decomposition (SVD) to recover an approximate IP by directly inverting a discretized convolution. This second technique is less constrained and therefore gives poorer results than NLLS, but is useful when the form of the IP is unknown. Using the NLLS technique, we demonstrate by example that the IP is a function of position in the format of cross-dispersed echelle spectrometers. We also compare our results with laser and thorium emission-line profiles. Finally, we present the IP for a range of positions in the format of the Hamilton echelle spectrograph at Lick Observatory and the HIRES echelle at the Keck 10-m telescope.

1. INTRODUCTION

The interpretation of spectroscopic data requires a model, which usually includes both the physics of the source and perturbations caused by the instrumentation. Information about the source is limited by how well instrumental perturbations are characterized. An ideal spectrometer would map all light of a particular wavelength to a unique location on the detector. In a real spectrometer, monochromatic light is mostly concentrated into a localized region, but some light is also spread elsewhere on the detector. The distortions introduced by a spectrograph may be conceptually divided into far-field scattered light and near-field smearing. The techniques described in this article are useful for characterizing the core of the IP out to about 1% of the peak. This information is crucial for addressing a wide variety of astrophysical problems, which in our case includes measuring precision radial velocities and analyzing spectral line shapes, but is certainly not limited to these applications. The far wings of the IP are also important in some situations, as when measuring the faint continuum in a source with bright emission lines. In these cases, other techniques (e.g., deep laser exposures) are better suited to precisely characterizing the wings of the IP. Henceforth, we will ignore any global contribution by the IP below about 1% of the peak, assuming this component has been removed.

Localized "smearing" of monochromatic light may be described as a convolution. In two-dimensional images, the kernel is called the point-spread function (PSF), whereas in one dimension, it is referred to as the IP. The shape of the IP is usually described by an assumed functional form (Gaussian or sinc, for example) and a single width parameter that depends on the size of the entrance slit of the spectrograph. Many processes affect the shape of the IP, including diffraction by the entrance slit and subsequent optical edges, temporally variable refraction by air (spectrograph seeing), design compromises and manufacturing imperfections in the optics, and scattering within transmission elements and by dust on optical surfaces. Thus, an actual spectrometer IP often has additional structure on top of the nominal Gaussian or sinc shape. The variations are particularly noticeable when a fast camera is employed to image the spectrum onto a detector, as is typical of cross-dispersed echelle spectrographs (Vogt 1987, for a design example).

The shape of the IP depends on the intensity distribution of the light incident on the camera, due to zonal aberrations in the spectrometer optics. Telescopes typically feed the spectrometer with a light cone that is uniformly illuminated, except where the secondary mirror and its support structure block the light. On the other hand, calibration lamps contain narrow, unobstructed filaments or cathodes which produce a different beam than does the telescope. Diffusers are commonly used to smooth the intensity distribution at the expense of throughput, but substantial brightness variations often remain. Differences in the angular intensity distribution of light entering the spectrograph change how the subsequent optics are sampled and lead to differences in the cumulative IP formed when separate light paths are focused at the detector. A similar effect may occur when the entire light cone entering the spectrograph tilts due to mechanical flexure of

[1]Research reported herein is based on data obtained at the Lick Observatory operated by the University of California and at the W. M. Keck Observatory operated jointly by the University of California and the California Institute of Technology.

[2]Also at Department of Physics and Astronomy, San Francisco State University, San Francisco, CA 94132.

the telescope or due to changes in optical alignment. Illumination variations can be reduced by placing at the collimator a restrictive mask that only passes portions of the beam common to all observing modes. Optical fiber feeds at the slit also help, but do not completely solve, the problem of consistent spectrograph illumination (Hunter and Ramsey 1992). Spectrographs that change orientation are subject to internal flexure, which changes the light path and hence the IP.

The optical path traversed by light in the spectrograph also depends on the wavelength of light. Zonal aberrations in the optics are the primary cause of IP variations, so IP shape is often a function of position at the detector. In the particular case of a cross-dispersed echelle, the IP usually depends on grating order number and also location within each other. If the grating and camera are fixed and the detector moves, then the IP will be associated with a particular wavelength. If the grating tilt is adjustable and the camera and detector are fixed (e.g., the Hamilton echelle at Lick), then the IP will to first order be associated with a particular column in the CCD. If the entire camera and detector system moves with respect to a fixed grating, then the IP will be primarily a function of location on the detector. Because the PSF often has considerable structure, the procedure used to reduce two-dimensional images into one-dimensional spectra will also affect the shape of the IP.

Since the nominal IP of a spectrometer is perturbed by all of the above-mentioned effects, techniques for determining the IP must be carefully designed and implemented. The IP should be measured in conditions that mimic as closely as possible the normal operating mode of the spectrometer. Moreover, the technique should be capable of quantifying "spatial variations" in the IP at different positions on the detector and temporal variations over the course of a night and on longer time scales. In Sec. 2, we describe and implement a technique that is our best effort to satisfy these design criteria. In Sec. 3, we describe a few other IP recovery techniques and compare the results to our preferred technique. The effects of pixelation and noise are also addressed. Finally, Sec. 4 contains our conclusions.

2. NLLS DETERMINATION OF ANALYTIC IP

We describe here an advance over the use of comparison lamps, lasers, and telluric lines to determine an IP. In this technique, a spectrum of a standard reference source is obtained with the spectrograph to be characterized. This observed spectrum is compared with the known *intrinsic* spectrum of the same source convolved with a parameterization IP. A nonlinear least-squares (NLLS) technique is used to adjust the parameters of the IP and to determine the analytic IP that best reproduces the observed spectrum.

2.1 Mathematical Description of the Spectrometer

Let $f(\lambda)$ be the intrinsic spectrum of light incident on the entrance aperture of a spectrograph. The spectrograph disperses the light according to wavelength, producing a spectrum, $g(x)$, at the detector, where x is a measure of position along the direction of dispersion. Various physical limitations (finite grating resolution, non-negligible aperture width, optical aberrations) cause light of a particular wavelength to be spread over a range in x. Nonetheless, we can construct a function, $\lambda(x)$, which associates each wavelength with its most likely position on the detector. The choice of whether $\lambda(x)$ refers to the peak or the centroid of the IP is arbitrary, as long as the same definition is used throughout the analysis. With these definitions, the behavior of the spectrograph can be described by a convolution of the form

$$g(x)=\int_{-\infty}^{\infty} f[\lambda(x')]\phi(x-x')dx', \tag{1}$$

where the kernel, $\phi(x-x')$, describes the unknown IP. The normalization of f is preserved by requiring that

$$\int_{-\infty}^{\infty}\phi(x-x')dx'=1. \tag{2}$$

In Eq. (1), $g(x)$ is a continuous function that describes the spectrum at every position along the detector. In practice, however, detectors are composed of discrete pixels, each of which records the integrated spectrum over a small range of x positions. We can label the pixels with indices, i, that run from 0 to $n-1$, where n is the total number of pixels along the detector. We also define $n+1$ positions, x_i, such that x_i and x_{i+1} bound pixel i. Ignoring second-order effects, such as the modulation transfer function and nonuniform quantum efficiency across a pixel, the "observed spectrum" is a sequence of n points given by

$$g_i=\int_{x_i}^{x_{i+1}} g(x)dx. \tag{3}$$

The intrinsic spectrum and the IP may be similarly binned into discrete samples, f_j and $\phi_{j-j'}$, though the sampling interval can and indeed should be finer. In particular, the values of x used in constructing f_j and $\phi_{j-j'}$ are chosen such that exactly q "subpixels" fit into each "oversampled" detector pixel. The zero point of j is selected such that pixel boundary i in the observed spectrum corresponds to pixel boundary $j=qi$ in the oversampled intrinsic spectrum. Since the IP generally falls below 1% of its peak intensity a few pixels away from center, for S/N<1000 we may assume $\phi_{j-j'}$ is zero for $|j-j'|>p$ and drop these terms from the sums that follow.

With these definitions, Eq. (1) may be *imprecisely* (see Sec. 3.2) recast as

$$g_i=\sum_{j=qi}^{q(i+1)-1}\left(\sum_{j'=j-p}^{j+p} f_{j'}\phi_{j-j'}\right), \tag{4}$$

which, for the case of "equal sampling" ($q=1$), reduces to

$$g_i=\sum_{j=i-p}^{i+p} f_j\phi_{i-j}. \tag{5}$$

This convolution may be performed explicitly or reformulated as products of Fourier or other integral transforms.

2.2 Choosing a Reference Source

We have used two different reference sources in our IP recovery technique, namely, the disk-integrated solar spec-

trum and a backlit I_2 absorption cell. Reference spectra of both sources have been obtained with the McMath FTS (Kurucz et al. 1984; Marcy and Butler 1992). The spectra have a resolution of 400,000, noise below 0.1%, and are available in digital form. Spectral regions contaminated by telluric absorption vary and must be ignored during the IP recovery process. Instrumental broadening and noise in these reference spectra can be ignored when determining the IP of spectrographs with substantially lower resolution, such as the echelles at Lick and Keck Observatories, described below.

The most generally useful reference source is the Sun because of its accessibility, stability, and well-distributed spectral lines. During the day, a disk-integrated solar spectrum may be obtained by pointing the telescope at the sky and collecting sunlight scattered by the Earth's atmosphere (yielding a "day-sky spectrum"). Alternatively, sunlight may be fed to the telescope by direct reflection from an out-of-focus surface near the primary (a dome, for example). At night, the Moon or an asteroid are often accessible. It is possible that incoherent scattering by the Earth's atmosphere may reduce the depths of absorption lines in day-sky spectra by 1%–2% (Edmonds 1978; Cochran and Trafton 1978). High-resolution studies by Hearnshaw (1977) and Lind and Dravins (1980) did not, however, detect any difference between the depths of absorption lines in lunar and day-sky spectra. We also detect no difference in our echelle spectra. If evidence is found for excess scattered light in observed solar spectra, then a scattered light term can easily be included as an additional parameter in the NLLS procedure.

Using the Sun or Moon as a reference source does have some drawbacks. The Moon is not always visible and asteroids are faint, so it is not always possible to monitor changes in the IP over the course of a night. Also, reflected solar light usually fill the field of view of the telescope, whereas observations of point sources do not. Such differences in how the spectrograph optics are illuminated lead to corresponding differences in the IP. A mask at the collimator can help ameliorate this problem.

An I_2 absorption cell provides an alternative IP reference source. A temperature-controlled I_2 cell is placed in the light path before the entrance slit of the spectrograph and overlays a molecular absorption spectrum on the astronomical target spectrum. The advantage of this technique is that the target spectrum and the IP information are obtained simultaneously and under exactly the same conditions of illumination. As an added bonus, the I_2 spectrum is much richer than the solar spectrum, providing much stronger constraints on the IP. On the down side, the IP can only be determined in the portions of the spectrum with molecular iodine bands (500–630 nm), though Cl_2, Br_2, $CSCl_2$, ClO_2, SO_2, and NO_2 provide useful band structure in other spectral regions (Butler 1987). Also, I_2 absorption lines are superposed on the astronomical source spectrum, so both spectra must be modeled together.

Figures 1 and 2 show representative spectra of the Sun and of an I_2 absorption cell. The various spectra were obtained with the Hamilton echelle at Lick Observatory, the McMath FTS, or synthesized from an FTS spectrum convolved our best guess for the Hamilton IP. The agreement between synthetic and actual Hamilton spectra is outstanding, as can be seen from the magnified residuals at the bottom of each figure. The high information content of the I_2 spectrum is also apparent. In time, high-quality atlases of bright, stable stars will also become available for use as IP reference spectra.

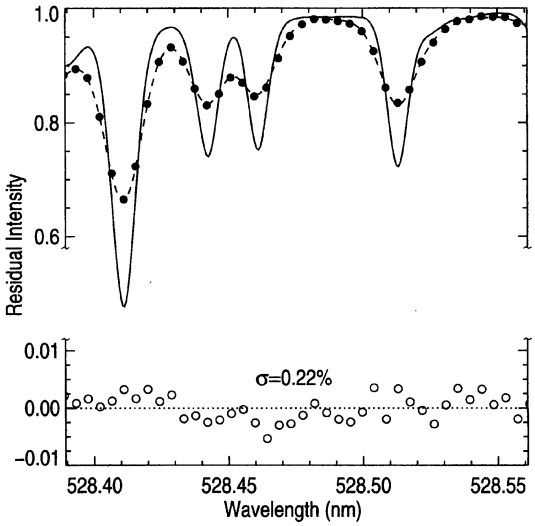

FIG. 1—Comparison of an FTS spectrum of the Sun (solid curve), a Lick Hamilton echelle spectrum of the Sun (filled circles), and a synthetic echelle spectrum (dashed curved) constructed from the NSO solar atlas and an inferred instrumental profile. The small difference between the synthetic and actual echelle spectra are shown (magnified by a factor of 10) at the bottom of the figure.

2.3 Parametrizing the IP

The analytic form of the IP must be selected with care. Too little flexibility in the function and the analytic IP will not be able to mimic the true IP. Too much flexibility and the

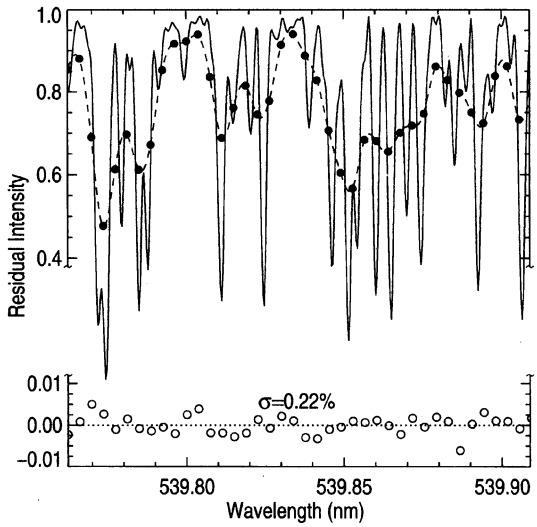

FIG. 2—Another demonstration of the good agreement between synthetic and actual Hamilton echelle spectra, as in Fig. 1, except that here, the source is an incandescent lamp viewed through an I_2 absorption cell.

analytic IP will permit noise-induced artifacts. We prefer to err on the side of too much flexibility. A fairly general functional form should be used initially, when the basic form of the IP is unknown. Subsequently, more restricted functional forms with fewer free parameters can be used to obtain a more precise IP. The greatest advantage of a well-chosen analytic form is its ability to constrain the final IP, but specifying the IP analytically also allows the IP to be sampled at arbitrary scales.

Since most IPs are approximately Gaussian or sinc, these functions provide the logical starting point for a functional specification. Simple Gaussians may be modified by allowing each wing to have a separate width, including Lorentzian or power-law wings, adding multiple Gaussians, using Gauss–Hermite polynomials (a suggestion by David Moore), and so on. Some of these functional forms have been used to describe the IP of the GHRS echelle (Cardelli et al. 1990) and the PSF in CCD images (Stetson et al. 1990). Hermite polynomials have been used successfully in modeling non-Gaussian line profiles of elliptical galaxies (Van der Marel and Franx 1993). A less-constrained (but still smooth) IP can be obtained by fitting a cubic spline through nodes with fixed locations and adjustable amplitudes. The wings of the spline are forced to zero by bracketing the IP with nodes set to zero.

For this article, we characterize the IP as the normalized sum of one central and four to eight satellite Gaussians. For markedly asymmetric IPs, one may place an extra Gaussian on the side with the extended wing. The centers of the Gaussians and the widths of the satellite Gaussians are set *a priori* for each spectrograph (and range of slit sizes). The free parameters in this specification of the IP are the amplitudes of the satellite Gaussians and the width of the central Gaussian. The amplitude of the central Gaussian is constrained by an overall normalization requirement. The widths of the satellite Gaussians are set so that their half-widths just overlap. This rather general functional form permits a Gaussian IP to have asymmetric, non-Gaussian wings, while maintaining general smoothness in the final IP. Variations on this functional form have proven to be equally successful. Once the range of IP shapes is known for a particular spectrometer, a more specific functional form may be selected, further reducing unwanted degrees of freedom.

2.4 Optimizing the IP by NLLS

We determine the IP by adjusting free parameters to yield optimal agreement between an observed spectrum (obtained with the spectrograph to be characterized) and a synthetic spectrum of the same source. The synthetic spectrum is generated by convolving a very high-resolution reference spectrum with an assumed IP and then rebinning the spectrum to match the pixel locations in the observed spectrum [see Eq. (4)]. The synthetic spectrum is then multiplied by a linear trend to match the observed spectrum, and fit quality is assessed. Improved values of IP and other free parameters are selected, and the process continues iteratively until χ^2 changes by less than 0.01%.

Since the IP generally depends nonlinearly on the IP parameters, a NLLS optimization algorithm is required. Several such algorithms are discussed by Press et al. (1986). We use the gradient-expansion technique developed by Marquardt (Press et al. 1986; Bevington and Robinson 1992), which has also been used previously to determine the PSF in crowded CCD fields (Mighell 1989). In most cases, the algorithm quickly approaches (but never quite reaches!) a minimum in χ^2. Caution is advised in using all such routines, however.

Other parameters can be varied in addition to the IP parameters. For example, the wavelength scale for the observed spectrum can be fixed or allowed to vary, depending on how well it is known. We typically allow both the dispersion and the wavelength zero point to vary. Although we solve separately (within each iteration) for the two parameters specifying the linear trend used to match the observed and synthetic spectra, they could easily be combined into the overall NLLS analysis. Scattered light should be removed prior to IP recovery, but it is nonetheless possible to include a scattered light parameter explicitly in the NLLS analysis.

To improve computational efficiency, the highly oversampled reference spectrum may be rebinned into coarser wavelength bins prior to use. Accurate rebinning can be done by fitting a cubic spline to the FTS spectrum and integrating numerically under the spline within each new wavelength bin. Monte Carlo tests indicate that at least four reference pixels are needed within each (Lick or Keck) echelle pixel ($q \geq 4$) in order to recover the true IP.

We use a conventional χ^2 statistic to optimize the fit. This is appropriate when the only source of error is normally distributed noise in the observed spectrum. Defective detector pixels, cosmic rays, and electronic noise may all give rise to anomalously bad pixel values ("outliers"). To obtain accurate results, outliers should be ignored when solving for IP parameters. Alternatively, a statistic more robust than χ^2 can be used, such as "M estimates" (Press et al. 1986; Branham 1990), but then the gradient-expansion algorithm will no longer work.

The weights assigned to each pixel in computing χ^2 can be estimated by adding in quadrature the predicted Poisson noise, detector read noise, uncertainties introduced by flat-fielding, etc. If for some reason the reference spectrum has significant noise compared to the observed spectrum being analyzed, then it may be desirable to artificially reduce the weights of continuum points. Such points carry no valid information about the IP, but do perturb the χ^2 surface, thereby introducing errors in the IP parameters. When the noise in the reference spectrum is negligible; as it is in the FTS spectra described above, no artificial weights should be applied to the noise estimates for each pixel. Any such weighting scheme throws away information and potentially biases χ^2.

2.5 Application to Keck and Lick Echelles

We have used the NLLS technique described above to study the instrumental profiles of the Hamilton echelle at Lick Observatory (Vogt 1987) and the HIRES echelle at Keck Observatory (Vogt 1992; Epps and Vogt 1993; Vogt et al. 1994). For nominal slit widths, both spectrometers have spectral resolving powers of approximately 5×10^4 with two-pixel sampling.

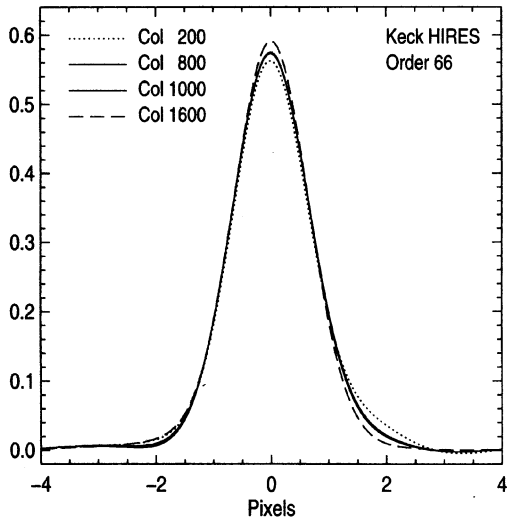

FIG. 3—Instrumental profiles determined by a NLLS analysis of 200 column segments of a Keck HIRES I_2 spectrum. Adjacent IPs agree well, while more distant IPs reveal the existence of spatial gradients. Asymmetries are also evident in the wings of the IP. The center of order 66 is at approximately 539.61 nm.

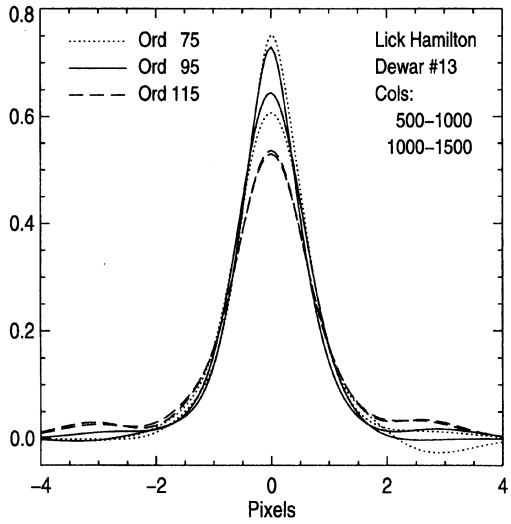

FIG. 4—Instrumental profiles determined from a NLLS analysis of 500 column segments of a Lick Hamilton day-sky spectrum obtained with the CAT. Variations in IP shape are seen as a function of both column and order, with a general increase in IP width towards the blue (higher-order number). Central wavelengths for orders 75, 95, and 115 are 761.84, 601.45, and 496.85 nm, respectively.

Lick observations were made with slit widths between 150 and 900 μm, where a slit width of 400 μm corresponds to 0.75 arcsec on the sky (with the 3-m telescope) and projects to 1.2 CCD pixels (Misch 1991). Refurbished imaging optics were installed in the Hamilton on 1994 November 1, yielding a significantly narrower and more symmetric intrinsic IP. Observations prior to this date were made with a 600 μm slit and were recorded with the 800×800 Texas Instruments CCD in Dewar No. 8. Post-refurbishment observations were made with narrower slits and were recorded with the 2048×2048 Ford Aerospace CCD in Dewar No. 13. Both CCDs have 15 μm pixels. Keck observations were made with a 417 μm slit, corresponding to 0.575 arcsec on the sky and 1.45 pixels on a Tektronics 2048×2048 CCD with 24 μm pixels.

An incandescent lamp shining through an I_2 absorption cell at 50 C was used as a reference source at both observatories. In addition, the day sky, as observed by the CAT, was used as a reference source at Lick Observatory. We used an IP comprised of multiple Gaussians, as described in Sec. 2.3. Each spectral order was broken into many 40 pixel segments, which were analyzed separately. With five to nine free IP parameters, two wavelength scale parameters, and two linear trend parameters, the fit to each chunk of spectrum typically had ν=27 degrees of freedom. Spectral segments with bad pixels or significant telluric absorption had fewer constraints. To improve IP accuracy, we often combined independent profiles in a region spanning several echelle orders and a few hundred CCD columns, rejecting highly discrepant profiles and fitting linear trends to variations with order and column number.

Figure 3 shows instrumental profiles at a few column locations in the Keck/HIRES spectrometer. The IPs for columns 700–900 and 900–1100 are nearly identical, indicating the high level of precision attainable with an I_2 reference source. In contrast, the IPs for columns 200 and 1600 show small but systematic differences, illustrating a common property of echelle spectrographs: spatial variability of the IP. Figure 3 also demonstrates another feature typical of echelle spectrographs: asymmetric wings in the IP. These unwanted distortions are almost inevitable, given the design compromises needed to image a large and very broadband echelle format achromatically onto a small CCD.

Figure 4 shows instrumental profiles derived from day-sky spectra for the refurbished Hamilton spectrometer. The IP becomes broader in the blue (higher-order numbers), as predicted by detailed ray tracing of the optical design (according to Steve Vogt, private communication). The index of refraction of glass changes more rapidly in the blue, so aspherical optics designed to cover the entire visible spectrum are usually optimized for uniformity at longer wavelengths. For order 115 ($\lambda\sim$496.85 nm), the two IPs at two locations along the spectral order are very similar, demonstrating again the high precision of our technique. Variations *within* orders 75 ($\lambda\sim$761.84 nm) and 95 ($\lambda\sim$601.45 nm) have the same sense (narrower IP at higher column numbers) and are due to changes in IP breadth along an order. The negative excursion in the wing of the IP for order 75 is an artifact that provides an estimate of possible errors in the IP. Precision decreases towards the red (lower-order numbers) as the number of solar lines (IP constraints) decreases.

Figure 5 illustrates how the IP of the refurbished Hamilton spectrometer broadens with increasing slit width. Instrumental profiles were determined from day-sky spectra, which uniformly illuminated the slit from the telescope exit pupil. We measured FWHM of 0.96, 1.22, 1.59, and 2.17 pixels for slit widths of 150, 400, 600, and 900 μm, respectively. Order

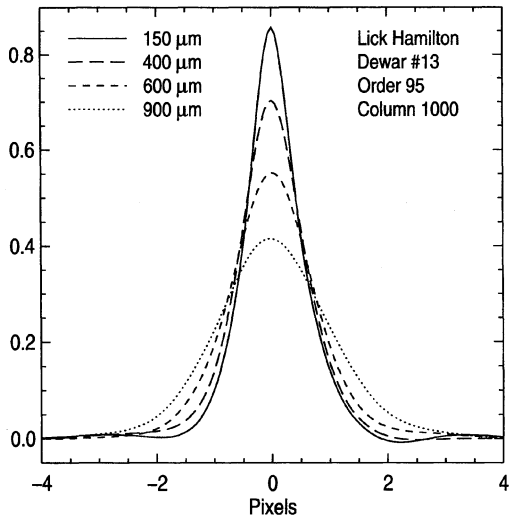

FIG. 5—Progression of instrumental profiles for the refurbished Hamilton echelle at Lick Observatory as slit width increases from 150 to 900 μm. In all cases, the slit was uniformly illuminated by the day sky observed with the CAT. The central wavelength for order 95 is 601.45 nm.

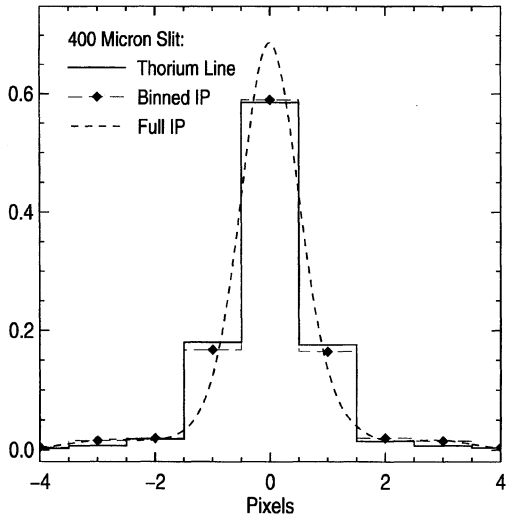

FIG. 6—Comparison of a thorium profile (solid histogram) and the NLLS IP (dashed curves) determined from a CAT day-sky spectrum obtained with the refurbished Hamilton spectrometer at Lick Observatory. The thorium line is slightly broader in the core than the binned IP (dashed histogram +diamonds). The thorium line is located in order 106 at column 1152 of Dewar No. 13 and has a wavelength of 539.476 nm.

95 has a central wavelength of 601.45 nm and each 15 μm pixel of Dewar No. 13 corresponds to 0.00494 nm, implying spectral resolving powers of 120,000, 98,000, 77,000, and 56,000 as a function of increasing slit width. The IP is undersampled for all but the widest slit width. As sampling decreases, the IP derived from a single line becomes progressively more uncertain. Even with sampling as poor as 1 pixel per resolution element, we succeed because we use a well-behaved analytic IP to analyze many spectral lines with basically random discrete positioning. Practical sampling requirements depend on the number of lines being analyzed and how well the intrinsic form of the IP is known. Observations of point sources in good seeing will illuminate the slit unevenly, yielding instrumental profiles that are narrower than those in Fig. 5. The inflection point in the red wing of the 150 μm IP is an artifact caused by the poor sampling of the narrow IP, coupled with a functional form for the IP designed for a broader IP.

3. COMPARISON WITH OTHER TECHNIQUES

3.1 IP Recovery from "Narrow" Lines

One common method of estimating the IP rests on the assumption that the IP is given by the shape of "narrow" spectral lines. Chosen lines are nearly monochromatic from a lamp or laser, but telluric absorption lines have also been used. This technique is only valid if the spectral lines are unresolved by the spectrograph and do not overlap. Moreover, the angular intensity distribution of light entering the spectrograph must match the corresponding distribution of light fed by the telescope during astronomical observations (see Sec. 1). In practice, it is difficult to obtain extensive IP information, while still satisfying these constraints.

Emission lines from Th–Ar or Fe–Ne lamps can be detectably broadened even at moderate resolution, due to Doppler broadening, pressure broadening, and blending. In Fig. 6, we compare a thorium line (539.476 nm) in order 106 of the refurbished Hamilton with the IP determined by an analysis of a day-sky spectrum. To facilitate the comparison, the finely sampled IP has been aligned and binned into synthetic Hamilton pixels. Although the profiles are close, the thorium line is slightly broader in the line core and slightly depressed in the wings. The difference may be due to actual broadening of the thorium line or it may be due to differences in the way the entrance cone of the spectrograph was filled by the lamp and the day sky. Differences are not always so subtle. Before the Hamilton was refurbished, zonal aberrations in the spectrometer were very pronounced and thorium lines were clearly broader than the IP. This serves as a practical reminder that one should not just assume that thorium lines are broadened by the same IP as are lines in astronomical spectra entering the spectrometer through the telescope.

Laser lines are unresolved, as are lines from microwave-excited isotopic Hg lamps (Griffin 1969; Gray 1992). With both of these sources, a diffuser must be used to provide uniform illumination of the spectrograph optics. A diffuser also destroys the coherence of light from the laser. Spectrometers act as mild polarizers, due to nonisotropic reflections from the grating and other optics. Thus, any calibration source, including that used to measure the IP, should have the same polarization characteristics as astronomical sources, lest the spectrometer response be affected differentially. Using an iodine cell to recover the IP will properly account for polarizing effects, since superposition of iodine lines does not affect the light path. In contrast, reflected sunlight must deflect off either air or a solid body, thereby introducing different polarization characteristics. The importance of this effect, which we have not attempted to measure, depends on

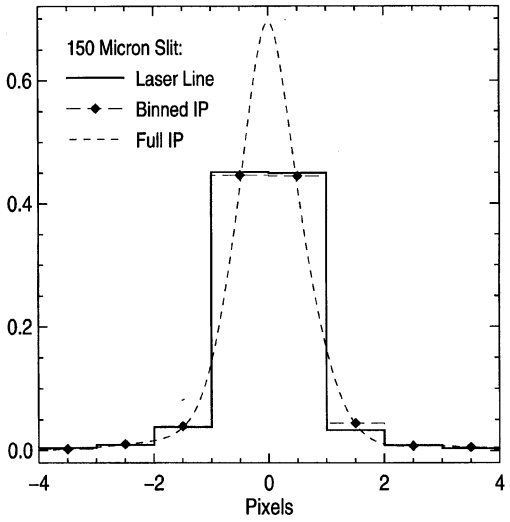

FIG. 7—Comparison of a laser profile (solid histogram) and the NLLS IP (dashed curves) determined from a CAT day-sky spectrum obtained with the refurbished Hamilton spectrometer at Lick Observatory. The laser line and binned IP (dashed histogram+diamonds) agree well, given the reduced slit width of only 150 μm. The laser line is located in order 90 at column 554 of Dewar No. 13 and has a wavelength of 632.817 nm.

the polarizing properties of the spectrometer and the day-sky source. In contrast to laser and thorium sources, the day-sky spectrum does include the polarization characteristics of the telescope. Nonetheless, lasers provide a potentially valuable (albeit localized) check of other more general IP recovery techniques.

In Fig. 7, we compare the Hamilton IP determined by our NLLS technique with a He–Ne laser profile at 632.817 nm. Both observations were made with a 150 μm slit, which projects to only 0.45 CCD pixels. The narrow slit challenges the integrity of the IP recovery technique, since the IP is sub-Nyquist sampled (FWHM$\approx$1.2 pixels). Nonetheless, the binned IP matches the observed laser line rather well. Discrepancies can easily be attributed to differences in spectrograph illumination. Unless the laser is tunable, it provides IP information at only one location in the spectrum, whereas the Hg lamp provides information at a few locations. More generally, iodine provides detailed IP information from 500 to 630 nm, while the Sun provides constraints on the IP at all wavelengths. These sources of IP information complement one another.

In order to accurately measure the shape of narrow emission lines, the response of the detector must be well calibrated over a large range of input signal, which can be difficult. For example, the charge transfer efficiency of a CCD is affected by local distortions in the electrostatic potentials within pixels. A sharp emission-line spectrum and a continuous spectrum of the Sun present very different charge-transfer environments, which may lead to different effective instrumental profiles. It cannot be stressed enough that the illumination characteristics of the IP reference source should match actual observing conditions as closely as possible.

Telluric O_2 absorption lines may also be used to determine the IP (Griffin 1969; Caccin et al. 1985), much as I_2 absorption lines are used in the NLLS technique. Illumination characteristics are identical for both the target and telluric spectra, which is good. Unfortunately, telluric lines depend on airmass and humidity. Moreover, they have non-negligible widths due to thermal and (height-dependent) pressure broadening, so generating a reference spectrum can be difficult (Caccin et al. 1985).

3.2 Singular Value Decomposition

The IP may also be determined by inverting Eq. (1) and solving for the IP directly. Equation (4) describes a system of n linear equations (constraints imposed by the n observed pixels) with $2p+1$ unknowns (the discretely sampled IP). The binned intrinsic spectrum, f_i, is assumed to be known, *a priori*. This system of equations may be rewritten in matrix form as

$$\mathbf{g}=A\,\phi, \tag{6}$$

where $\mathbf{g}=\{g_i\}$ for $i=[0,n-1]$, and $\phi=\{\phi_k\}$ for $k=[-p,p]$. Elements in A are given by

$$a_{ik}=\sum_{l=0}^{q-1} f_{qi+k+l+p}, \tag{7}$$

for an oversampled IP, or simply $a_{ik}=f_{i+k+p}$ for equal sampling.

This gives the system of linear equations in Eq. (6), where $\mathbf{g}$ is the observed spectrum and A is constructed from the intrinsic spectrum. This system of equations (usually) overconstrains the IP (ϕ), and an optimum solution is found by minimizing the χ^2. Equation (6) follows from Eq. (1) only if both the IP and the intrinsic spectrum are step functions, i.e., constant within each pixel. Since this condition is false, Eq. (6) is only an approximation. The error incurred by making this approximation may be reduced by increasing the IP oversampling parameter (q). Equation (6) is solved using singular value decomposition (SVD), which is preferred over ordinary least-squares methods (Press et al. 1986) because it minimizes fluctuations in the IP due to noise.

Figure 8 shows instrumental profiles determined for three adjacent 40 pixel segments of the Lick Hamilton format in four consecutive I_2 absorption spectra. The three IP recovery techniques that are compared are SVD with no oversampling of the Hamilton pixels ($q=1$, unfilled circles), SVD oversampled by a factor of 2 ($q=2$, filled squares), and NLLS (solid curves). Overall, SVD profiles agree quite well with the results of the NLLS analysis, but SVD profiles are much noisier. Small differences in the profiles for consecutive iodine spectra illustrate the extent to which noise in a single exposure affects the results.

3.3 Effects of Pixelization

While the SVD profiles agree with the NLLS profiles on average, any particular pixel is systematically in error. This is primarily due to a breakdown of the approximation made in discretizing the convolution equation. Even with an oversampling of two (which gives nearly as many IP points as observed pixels), there is substantial structure in the iodine spectrum within one oversampled pixel (see Fig. 2).

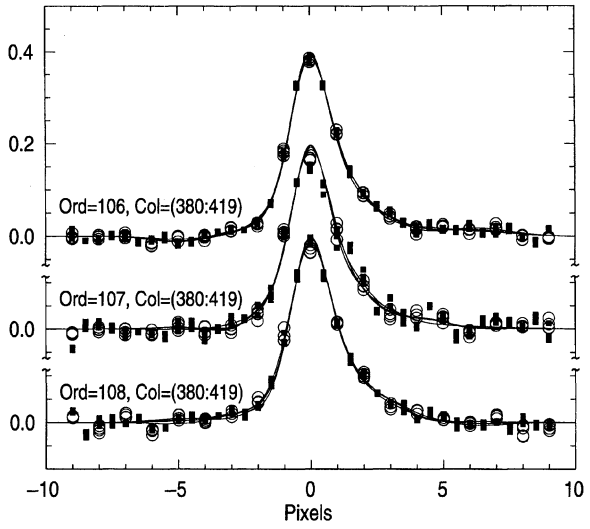

FIG. 8—Comparison of instrumental profiles determined from three adjacent regions in four consecutive echelle spectra. The instrumental profiles recovered using NLLS (solid curves) all agree quite well with one another. Profiles determined from SVD (unfilled circles) and 2×SVD (filled squares) agree with the results of NLLS on average, but show systematic errors in individual pixels, due to limited sampling.

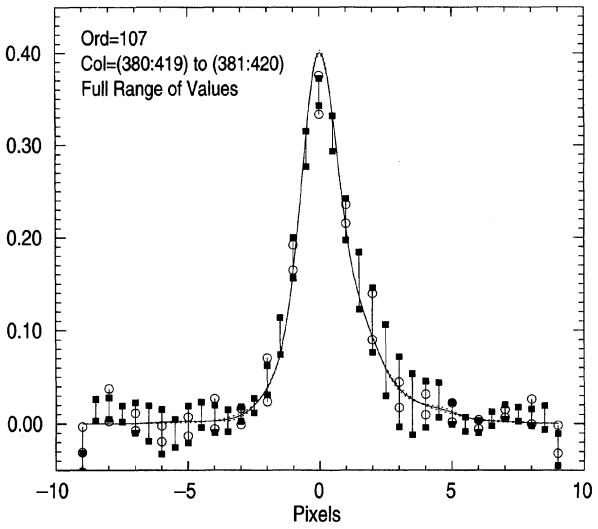

FIG. 9—Results of a numerical experiment studying how the recovered IP is affected by binning into CCD pixels. A segment of I_2 spectrum was convolved with an assumed IP (solid curve), binned into synthetic CCD pixels, and then analyzed to recover an IP. The alignment of the synthetic pixels was shifted successively by 0.05 pixels for a sequence of 21 trials. The full range of recovered IPs are shown for the NLLS (dashed curves), SVD (unfilled circles), and 2×SVD (filled squares) recovery techniques. The SVD techniques are much more prone to error.

To illustrate this point, Fig. 9 shows the results of a numerical experiment in which the intrinsic iodine spectrum was convolved (on a very fine pixel scale) with the solid curve in the figure (an assumed IP) and numerically binned into synthetic Hamilton pixels (with no noise added). The alignment of the Hamilton pixels initially matched the alignment of the actual observations in Fig. 8. The alignment of the synthetic pixels was then shifted by 0.05 pixels and a new IP was determined. The process continued until a shift of one full pixel was reached.

Figure 9 shows the range of values that were systematically traversed by each point in the IP. Even though the spectral segments contained nearly identical information and no noise for each of the 21 trials, each location in the SVD profiles varies significantly. The dashed lines show the full range of curves deduced with the NLLS method, which obviously fared much better. From Fig. 8 it is clear that the error due to noise in a well-exposed Hamilton spectrum is substantially smaller than the error due to discrete sampling.

3.4 Noise in the Observed Spectrum

A simple Monte-Carlo experiment illustrates how the deduced IP is affected by noise in the observed spectrum. First, a synthetic Hamilton spectrum is generated by convolving a segment of the FTS iodine spectrum with the appropriate IP for the Hamilton, and binning the result to the Hamilton pixel scale. Then, Gaussian noise with a standard deviation of 0.1%, 0.33%, 1%, or 3.3% is added to the spectrum, and the result is used to recover an IP, as if the spectrum had actually been observed with the Hamilton. The process is repeated 100 times with different noise for each trial. The spectrum is also analyzed with no noise added.

Figure 10 shows the range of instrumental profiles determined in such an experiment. Points connected by a line indicate $\pm 1\sigma$ variations in the profiles derived by SVD using the Hamilton pixel scale (unfilled circles) or an oversampled pixel scale ($q=2$, filled squares). For low noise cases, the $\pm 1\sigma$ points overlap. The threshold for setting SVD pivots to zero was not tuned for the low S/N case, so results slightly

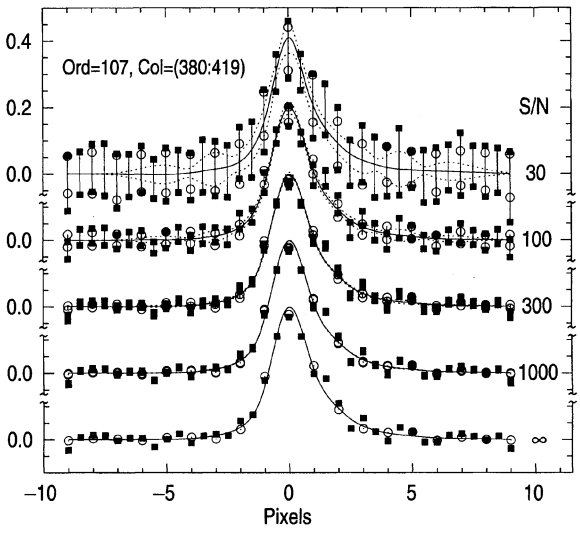

FIG. 10—Results of a Monte-Carlo experiment studying how the recovered IP depends on noise in the original spectrum. A segment of I_2 spectrum was convolved with an assumed IP (solid curves) and binned into synthetic CCD pixels. After adding Gaussian noise, the spectrum was analyzed to recover an IP. The full range of recovered IPs are designated by symbols as in Fig. 9.

TABLE 1
Hamilton Spectrograph Instrumental Profiles (400 μm Slit)

	Based on Solar Spectrum															Based on I_2 Spectrum		
	Order 75			Order 85			Order 95			Order 105			Order 115			Order 105		
Pixel	500	1000	1500	500	1000	1500	500	1000	1500	500	1000	1500	500	1000	1500	500	1000	1500
−5.00	0	0	−1	0	1	7	0	0	0	0	0	0	1	1	1	0	0	0
−4.75	0	0	−1	0	0	7	0	0	0	1	0	0	2	3	2	1	1	1
−4.50	0	−1	−4	0	0	8	1	0	1	1	1	1	5	6	5	2	2	2
−4.25	0	−1	−8	−1	−2	8	2	0	2	3	2	2	10	12	11	5	5	5
−4.00	−1	−2	−15	−2	−5	10	4	−1	3	6	4	4	18	22	19	10	9	10
−3.75	−2	−2	−25	−3	−9	12	6	−1	4	10	7	7	28	34	29	18	15	17
−3.50	−3	−3	−36	−5	−14	16	10	−1	6	15	11	10	38	46	41	27	23	26
−3.25	−4	−3	−46	−8	−18	23	14	−1	9	20	15	15	45	54	50	36	31	35
−3.00	−3	−4	−50	−9	−21	31	16	1	11	24	18	19	47	55	54	43	37	41
−2.75	0	−5	−44	−9	−20	41	17	4	14	25	20	22	44	49	53	45	39	43
−2.50	6	−5	−28	−6	−14	50	17	8	17	24	20	26	40	41	51	43	37	41
−2.25	15	−2	−3	1	−2	58	16	13	21	23	19	30	41	37	52	39	34	36
−2.00	30	9	28	15	18	63	20	22	29	25	20	36	55	47	65	38	32	33
−1.75	52	32	64	38	48	62	35	35	40	34	26	46	86	76	93	43	35	33
−1.50	86	67	98	77	93	57	67	59	56	55	41	61	133	125	137	62	46	44
−1.25	144	119	131	145	162	60	128	108	84	103	79	95	200	198	200	111	79	84
−1.00	253	205	184	268	272	112	245	206	152	207	167	178	308	313	305	225	172	186
−0.75	440	357	316	463	445	264	438	372	302	397	339	348	483	492	482	427	361	382
−0.50	686	586	575	708	679	535	690	605	553	657	599	608	714	720	715	684	634	653
−0.25	909	847	875	920	906	850	914	865	847	899	875	878	919	919	920	907	892	900
0.00	1000	1000	1000	1000	1000	1000	1000	1000	1000	1000	1000	1000	1000	1000	1000	1000	1000	1000
0.25	912	876	862	910	897	836	903	853	857	901	871	874	917	921	915	916	898	901
0.50	696	631	604	702	673	534	688	587	570	659	602	609	715	720	712	687	646	661
0.75	450	394	375	472	440	296	458	359	319	399	351	364	487	493	490	414	370	400
1.00	252	229	226	290	262	154	276	200	162	210	185	204	310	314	320	202	173	210
1.25	131	140	147	174	145	82	154	105	84	106	98	120	195	194	212	87	73	108
1.50	70	94	105	105	73	46	80	55	50	58	56	74	124	119	145	40	36	62
1.75	42	59	79	64	30	27	36	30	31	36	33	46	84	77	106	26	24	39
2.00	30	28	59	41	6	19	11	21	20	26	22	29	67	62	87	25	23	29
2.25	28	3	44	30	−7	19	−2	21	14	23	19	21	64	62	79	31	28	29
2.50	28	−14	32	23	−12	23	−7	24	11	24	20	20	64	66	74	37	34	34
2.75	28	−23	22	17	−13	28	−8	26	10	24	22	21	60	64	65	41	37	39
3.00	25	−25	14	12	−11	29	−7	25	9	22	22	20	50	55	52	39	35	38
3.25	21	−22	9	8	−9	27	−5	21	8	18	18	16	37	42	38	32	29	32
3.50	16	−17	5	4	−6	23	−3	16	6	13	13	12	24	28	25	23	21	23
3.75	11	−11	3	2	−3	19	−2	10	4	8	9	8	14	16	14	14	13	15
4.00	7	−7	2	1	−2	14	−1	6	2	5	5	4	7	8	7	8	7	8
4.25	4	−4	1	1	0	11	−1	3	1	2	2	2	3	4	3	4	3	4
4.50	2	−2	1	0	0	9	0	2	1	1	1	1	1	2	1	2	1	2
4.75	1	−1	0	0	0	8	0	1	0	0	0	0	0	1	0	1	1	1
5.00	0	0	0	0	1	7	0	1	0	0	0	0	0	0	0	0	0	0

better than those presented here are possible. The solid line shows the assumed IP, and the dotted lines show the $\pm 1\sigma$ ranges for the profiles determined using the NLLS method. Uncertainties in the NLLS profiles are largest at the positions of the satellite Gaussians, since our particular IP formulation has the greatest freedom at these points. As indicated in the earlier tests, instrumental profiles recovered by SVD have more noise as well as a systematic error in individual pixels, due to inadequate sampling. Figure 10 also demonstrates that S/N of at least 300 is desirable in order to accurately recover the IP (at least for only 40 observed pixels and an information-rich reference source, such as iodine). Uncertainty in the derived IP scales as $1/\sqrt{N}$, where N is the number of spectral lines containing IP information.

3.5 Fourier Deconvolution

Equation (5) may also be inverted using discrete Fourier transforms. Although Fourier techniques are ubiquitous, they have some practical problems. Fourier techniques assume that the functions being deconvolved are continuous across their endpoints. This is fine for the IP, which goes to zero in both wings, but is not in general true of the reference spectrum. Padding the ends reduces Fourier ringing in a convolution, but there is no analogous operation in a deconvolution. Also, the continuous Fourier series fit to the observed spectrum does not reproduce the observed spectrum when integrated over pixels. This problem can be significant, since spectrographs are typically Nyquist sampled. Spectral lines in the Fourier representation are smoothed, leading to a broader inferred IP.

The most serious problem, however, is that even very small amounts of noise in the observed spectrum systematically broaden the derived IP. Noise preferentially affects the high-frequency components, which contain most of the IP information (again because spectrographs are usually Nyquist sampled). An optimal (Wiener) filter suppresses the high-frequency components at the expense of smoothing and broadening the deconvolved IP.

4. CONCLUSIONS

We have presented a NLLS technique whereby the parameters of an analytic function describing the instrumental profile of a spectrograph are ascertained by comparing newly observed and FTS reference spectra of a canonical source. The effectiveness of this technique has been demonstrated with both the Sun and an I_2 absorption cell as reference sources, giving instrumental profiles that are internally self-consistent and in suitable agreement with the results of other

TABLE 2
HIRES Instrumental Profiles: Order 66, Decker B2

Pixel	500	1500	Pixel	500	1500
−5.00	0	0	5.00	0	0
−4.75	0	0	4.75	0	0
−4.50	0	0	4.50	−1	0
−4.25	0	0	4.25	−1	0
−4.00	1	1	4.00	−2	−1
−3.75	1	1	3.75	−4	−1
−3.50	2	2	3.50	−5	−1
−3.25	3	2	3.25	−4	0
−3.00	4	3	3.00	−2	3
−2.75	5	5	2.75	2	7
−2.50	9	10	2.50	8	14
−2.25	20	26	2.25	18	23
−2.00	48	61	2.00	34	40
−1.75	99	124	1.75	64	71
−1.50	176	212	1.50	121	129
−1.25	278	320	1.25	220	231
−1.00	413	455	1.00	376	398
−0.75	589	625	0.75	581	615
−0.50	785	807	0.50	792	824
−0.25	940	945	0.25	946	961
0.00	1000	1000	—	—	—

more limited IP recovery techniques. Our analysis of data from both Lick and Keck Observatories demonstrates that the instrumental profile of an echelle spectrometer can be asymmetric and also spatially variable. This result underscores the importance of techniques, such as the one presented here, which can be used to map variations in the IP out to about 1% of the peak, as a function of position in the spectrograph. Radial-velocity measurements may be easily incorporated into the IP retrieval procedure by including the stellar Doppler shift as an additional free parameter in the NLLS analysis. This technique has been successfully employed to obtain Doppler measurements precise to 3 m s^{-1} (Marcy and Butler 1994).

We would like to acknowledge Chris Johns, Gibor Basri, Ron Gilliland, Steve Vogt, and Tim Brown for helpful comments. This work was supported by NASA Grant NAGW-3182.

APPENDIX: TABULATED INSTRUMENTAL PROFILES

A. Lick Hamilton Spectrograph

Using the NLLS technique described in this article, we have determined a set of instrumental profiles for the Hamilton echelle spectrometer at the Coudé foci of the 3-m and CAT telescopes at Lick Observatory. The instrumental profiles are listed one per column in Table 1 for certain echelle orders and CCD columns. We emphasize that *the precise shape of the IP is a function of time, spectrograph configuration, and observing conditions*, so these profiles should only be used when more appropriate IP data are unavailable. Nonetheless, the table does provide approximate instrumental profiles that will occasionally be of use. The Schmidt camera that images Hamilton spectra onto the CCD was refurbished on 1994 November 1, yielding a substantially narrower and more symmetric IP. Data obtained prior to this refurbishment should *not* be analyzed using the instrumental profiles in Table 1. Data from the original Hamilton optics were used to make Figs. 1, 2, 8, 9, and 10.

Peaks of the instrumental profiles in Table 1 have been normalized to 1000 to make it easier to intercompare profiles and to assess the decline in the wings. The profiles should be renormalized to unit area prior to use in a convolution in order to preserve spectrum normalization. It may also be necessary to reflect the IP about its center, depending on the behavior of the convolution routine used. Negative pixel offsets in the first column of Table 1 map to bluer wavelengths than the positive pixel offsets. The first five groups of instrumental profiles were determined from daytime spectra of scattered sunlight obtained with the CAT. The last group of profiles were determined from a spectrum of Regulus (HR 3982, B7 V, $v \sin i = 327$ km s^{-1}) obtained through an I_2 absorption cell, using the 3-m telescope. Differences between the solar and I_2 instrumental profiles for order 105 are probably due to differences in slit illumination and optical path (3 m vs. CAT). The negative excursions in some of the IP wings are almost certainly artifacts. The amplitude of these excursions indicates the uncertainty in the tabulated instrumental profiles, with lower precision for lower-order numbers due to the decrease in the number of spectral lines (IP constraints) in the Solar spectrum towards redder wavelengths.

Pixel numbers at the top of each column of Table 1 correspond to unbinned and unwindowed pixel numbers for the Ford Aerospace 2048×2048 CCD inside Dewar No. 13. Pixels are approximately 15 μm square. Note that for a given echelle order, the Hamilton IP is best characterized as a function of detector location, rather than wavelength. This is because each location on the detector corresponds to a particular light path through the camera (and hence a particular IP), whereas light of a particular wavelength can traverse the camera in a variety of ways, depending on the adjustable orientation of the echelle grating. The opposite is true of variations in the IP as a function of echelle order, since order selection done by translating the detector, rather than adjusting the tilt of the echelle grating. See Vogt (1987) for a more detailed description of the spectrograph. For reference, the central wavelengths of echelle orders 75, 85, 95, 105, and 115 of the Hamilton are 7618.4, 6722.1, 6014.5, 5441.7, and 4968.5 Å, respectively (Misch 1991).

Each IP in Table 1 is based on information contained in eleven echelle orders and 501 columns centered on the specified position. Observations were made with a slit width of 400 μm, which corresponds to 0.755 arcsec on the sky for the 3-m and 3.77 arcsec for the CAT. The entrance aperture of the spectrograph was uniformly illuminated for the solar observations with the CAT and very nearly so for the stellar observation with the 3 m. For slit widths larger than roughly 0.75 arcsec, slit illumination (and hence the shape of the IP) depends on both seeing and placement of the target on the slit. In this situation, it is especially useful to use an absorption cell in the beam to simultaneously determine the IP for each exposure. A slit with a width of 400 μm contributes significantly to the width of the IP, so that the intrinsic instrumental profiles of the spectrograph are narrower than

those in the table. In fact, tests with a 150 μm slit indicate that the intrinsic spectral resolving power of the refurbished Hamilton is at least 120,000 (see Sec. 2.5).

B. Keck HIRES Spectrograph

Table 2 contains instrumental profiles for the HIRES spectrometer fed by the 10-m telescope at Keck Observatory. As in Table 1, the peak of the IP has been normalized to 1000. Instrumental profiles were determined from an I_2 absorption spectrum superposed on a spectrum of 107 Piscium (HR 493, K1 V). The observations were obtained on 1994 November 24 with slit B2, which projects to 0.574 arcsec on the sky and 2.0 pixels at the detector. The observations were made approximately 2 hr from the meridian, which may influence the IP, due to the irregularly shaped pupil of the Keck telescope. As with the tabulated Hamilton IPs, we emphasize that *the precise shape of the IP is a function of time, spectrograph configuration, and observing conditions*, so these profiles should only be used when more appropriate IP data are unavailable. Moreover, these HIRES instrumental profiles cover only a limited portion of the echelle format around order 66 (central wavelength of 539.6 nm). More detailed IP maps will be published as data become available.

REFERENCES

Bevington, P. R., and Robinson, D. K. 1992, Data Reduction and Error Analysis for the Physical Sciences, 2e, (New York, McGraw-Hill), p. 161

Branham, Jr., R. L. 1990, in Errors, Bias and Uncertainties in Astronomy, ed. C. Jaschek and F. Murtagh (Cambridge, Cambridge University Press), p. 171

Butler, R. P. 1987, Master's Thesis, San Francisco State Univ., A Precision Astronomical Instrument to Measure Doppler Shifts, p. 16

Caccin, B., Cavallini, F., Ceppatelli, G., and Righini, A. 1985, A&A, 149, 35

Cardelli, J. A., Ebbets, D. C., and Savage, B. D. 1990, ApJ, 365, 789

Cochran, W. D., and Trafton, L. M. 1978, ApJ, 219, 756

Edmonds, F. N. 1978, PASP, 90, 322

Epps, H. W., and Vogt, S. S. 1993, Appl. Opt., 32, 6270

Griffin, R. F. 1969, MNRAS, 143, 319

Gray, D. F. 1992, The Observation and Analysis of Stellar Photospheres (Cambridge, Cambridge University Press), p. 253

Hearnshaw, J. B. 1977, PASP, 89, 356

Hunter, T. R., and Ramsey, L. W. 1992, PASP, 104, 1244

Kurucz, R. L., Furenlid, I., Brault, J., and Testerman, L. 1984, National Solar Observatory Atlas No. 1 (Tucson, NSO)

Lind, J., and Dravins, D. 1980, A&A, 90, 151

Marcy, G. W., and Butler, R. P. 1992, PASP, 104, 270

Marcy, G. W., and Butler, R. P. 1994, Eighth Cambridge Workshop: Cool Stars, Stellar Systems, and the Sun (San Francisco, ASP)

Mighell, K. J. 1989, MNRAS, 238, 807

Misch, A. 1991, Lick Observatory Technical Report No. 58, The Hamilton Spectrograph User's Manual (Santa Cruz, University of California)

Press, W. H., Flannery, B. P., Teukolsky, S. A., and Vetterling, W. T. 1986, Numerical Recipes (Cambridge, Cambridge University Press), p. 19

Stetson, P. B., Davis, L. E., and Crabtree, D. R. 1990, CCD's in Astronomy, ASP Conf. Series No. 8 (San Francisco, ASP), p. 289

Van der Marel, R. P., and Franx, M. 1993, ApJ, 407, 525

Vogt, S. S. 1987, PASP, 99, 1214

Vogt, S. S. 1992, in ESO Workshop on High Resolution Spectroscopy with the VLT (Garching, ESO), p. 223

Vogt, S. S., et al. 1994, Proc. Soc. Photo-Opt. Instr. Eng., 2198, 362